Cancer Cell
Article

Bacterially Derived 400 nm Particles for Encapsulation and Cancer Cell Targeting of Chemotherapeutics

Jennifer A. MacDiarmid,[1] Nancy B. Mugridge,[1] Jocelyn C. Weiss,[1] Leo Phillips,[1] Adam L. Burn,[1] Richard P. Paulin,[1] Joel E. Haasdyk,[1] Kristie-Ann Dickson,[1] Vatsala N. Brahmbhatt,[1] Scott T. Pattison,[1] Alexander C. James,[1] Ghalib Al Bakri,[1] Rodney C. Straw,[2] Bruce Stillman,[3] Robert M. Graham,[4,5] and Himanshu Brahmbhatt[1,*]

[1] EnGeneIC Pty Ltd, 105 Delhi Road, North Ryde, Sydney, NSW 2113, Australia
[2] Brisbane Veterinary Specialist Centre, Cnr. Old Northern Road and Keong Road, Albany Creek, Queensland 4035, Australia
[3] Cold Spring Harbor Laboratory, 1 Bungtown Road, Cold Spring Harbor, NY 11724, USA
[4] Victor Chang Cardiac Research Institute, 384 Victoria Street, Darlinghurst, NSW 2010, Australia
[5] School of Biotechnology and Biomolecular Sciences, University of New South Wales, Kensington, NSW 2054, Australia
*Correspondence: hbrahmbhatt@engeneic.com
DOI 10.1016/j.ccr.2007.03.012

SUMMARY

Systemic administration of chemotherapeutic agents results in indiscriminate drug distribution and severe toxicity. Here we report a technology potentially overcoming these shortcomings through encapsulation and cancer cell-specific targeting of chemotherapeutics in bacterially derived 400 nm minicells. We discovered that minicells can be packaged with therapeutically significant concentrations of chemotherapeutics of differing charge, hydrophobicity, and solubility. Targeting of minicells via bispecific antibodies to receptors on cancer cell membranes results in endocytosis, intracellular degradation, and drug release. This affects highly significant tumor growth inhibition and regression in mouse xenografts and case studies of lymphoma in dogs despite administration of minute amounts of drug and antibody; a factor critical for limiting systemic toxicity that should allow the use of complex regimens of combination chemotherapy.

INTRODUCTION

Severe toxicity remains a major factor limiting cancer chemotherapeutics. Lack of cancer cell specificity, indiscriminate drug distribution, and rapid clearance necessitate frequent administration of high doses of chemotherapeutics to elicit a satisfactory clinical response (Langer, 1998). Anticancer antibodies directed to overexpressed receptors on cancer cells, such as the epidermal growth factor receptor (EGFR; Nicholson et al., 2001) and HER2/*neu* (Rae and Lippman, 2004), are less toxic but do not possess the potency and wide spectrum antitumor activity of chemotherapeutic drugs. Efforts are being made to develop targeted drug delivery systems (DDSs), such as stealth liposomes (Medina et al., 2004), nanoparticles (Brannon-Peppas and Blanchette, 2004; Ferrari, 2005), and polymer therapeutics (Duncan, 2003), which encapsulate the cytotoxic drug in a vehicle and target it to cancer cells via tumor cell-surface receptors. However, these technologies are also hampered by shortcomings, such as drug leakage in vivo, lack of versatility in terms of packaging a diverse range of different drugs without significant derivatization, thereby reducing drug potency, and difficulties in production scale-up, particularly for nanoparticles.

Here we show that bacterial minicells which are anucleate nanoparticles produced as a result of inactivating

SIGNIFICANCE

Nontargeted cancer chemotherapy is currently associated with severe toxicity. This report describes bacterially derived nano-sized particles (minicells) for encapsulation of a range of different chemotherapeutic drugs and specifically targeting the minicells to tumor cell-surface receptors via bispecific antibodies coating the minicells. Receptor engagement results in minicell endocytosis, intracellular degradation, and drug release. Consequently, highly significant tumor growth inhibition and regression is achieved despite administration of minute amounts of drug and antibody. The dramatic increase in therapeutic index may permit the use of multidrug combinations to achieve an improved outcome for cancer therapy.

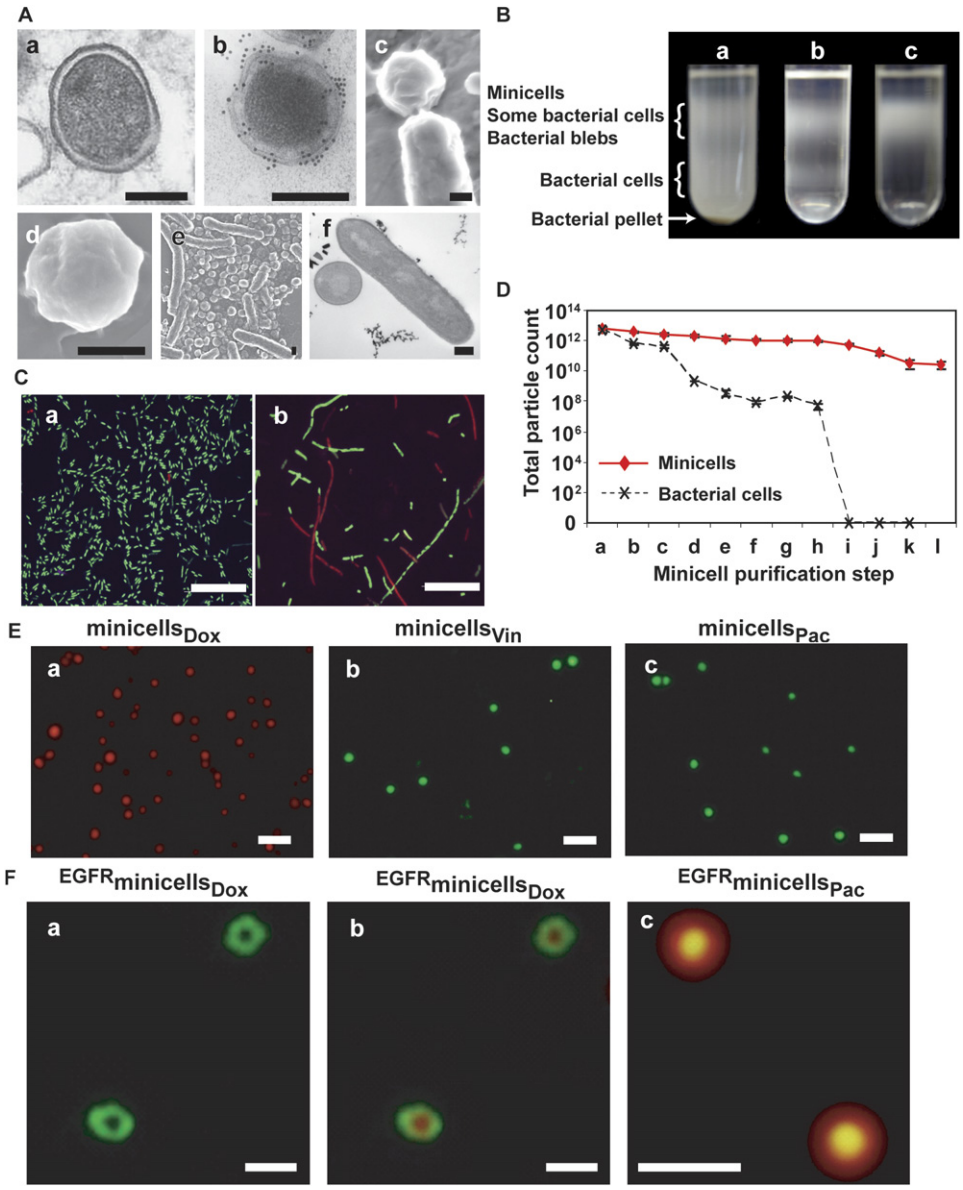

Figure 1. Minicell Characterization, Purification, Chemotherapeutic Drug Packaging, and BsAb Targeting

(A) Transmission (Aa, Ab, and Af) and scanning electron microscopy (Ac–Ae) of minicells derived from, *S.* Typhimurium showing inner and outer membrane structure (Aa), *S.* Typhimurium with immunogold labeling of surface O-antigen (Ab), minicell budding off parental *E. coli* (Ac), *S. flexneri* minicell and a mix of bacteria and minicells showing relative sizes and abundance (Ad and Ae), and *L. monocytogenes* minicell and parent cell (Af). Scale bar, 200 nm.

(B) Minicell purification using sequential density gradient centrifugation steps (Ba–Bc) on OptiPrep (6%–20% gradients) showing progressive separation and elimination of parental bacteria from the crude minicell preparation (Ba), resulting in significant purification by the third step (Bc).

(C) Fluorescence microscopy images showing differences in size between native *E. coli min*CDE- strain grown in the absence of NaCl (Ca), and filamentous forms stained with LIVE/DEAD Baclight bacterial viability kit (Molecular Probes; green [live], red [dead] fluorescence) resulting from growth in 5% NaCl (Cb). Scale bar, 20 μm.

(D) Minicell and bacterial counts during the various steps of minicell purification. (Da) overnight culture, (Db) differential centrifugation, (Dc) 0.45 μm crossflow filtration, (Dd–Df) successive OptiPrep gradients, (Dg) 2 hr activation of residual bacteria in TSB, (Dh) 2 hr incubation in TSB/5% NaCl, (Di) antibiotic treatment, (Dj) buffer exchange, (Dk) 0.45 μm dead-end filtration, (Dl) antiendotoxin treatment. Each value is a mean of three samples collected from a separate purification process. Error bars; ± SEM.

(E) Minicells packaged with Dox, showing red autofluorescence of the drug (Ea), or green fluorescence after loading with either BODIPY FL-conjugated vinblastine (Eb), or Oregon Green 488-conjugated Pac (Ec). No autofluorescence was observed with empty minicells (data not shown). Scale bar, 5 μm.

(F) Fluorescent images showing BsAb bound to and coating the surface of drug-packaged minicells. Alexa Fluor 488-conjugated BsAb (green fluorescence) bound to minicells$_{Dox}$ and imaged to show only the green fluorescence of the BsAb (Fa), or to show both the green fluorescent BsAbs, and

the genes that control normal bacterial cell division (De Boer et al., 1989; Lutkenhaus and Addinall, 1997; Ma et al., 2004), thereby derepressing polar sites of cell fission, may provide a solution to these and other obstacles to cytotoxic drug delivery.

RESULTS

Minicell Generation, Characterization, and Purification

Genetically defined *min*CDE− chromosomal deletion mutants were generated from *Salmonella enterica* serovar Typhimurium (*S*. Typhimurium), *Escherichia coli*, *Shigella flexneri*, *Pseudomonas aeruginosa* (Gram−), and *Listeria monocytogenes* (Gram+) strains. All mutants yielded large numbers of minicells with a uniform diameter of 400 ± 20 nm (Figure 1A). Like parental bacteria, minicells from Gram− bacteria have a ruffled surface (Figures 1Ac–1Ae) characteristic of their lipopolysaccharide (LPS) coat. By contrast, those from *L. monocytogenes* have the rigid cell-wall structure (Figure 1Af) expected of a Gram+ bacterial cell wall. That minicells are derived from their respective parental bacteria is evident, for example, by the ability to immunogold label *S.* Typhimurium minicells using an anti-*S.* Typhimurium O-antigen MAb (Figure 1Ab).

Complete and reproducible purification of minicells was achieved using a procedure to eliminate contaminants such as parent bacterial cells, cellular debris, intracellular components, free nucleic acids, and free endotoxin. Initial centrifugation and crossflow filtration steps (Figure 1B) resulted in >90% elimination of bacterial cells. However, some bacterial cells permeated the filter pores irrespective of how many serial crossflow filtrations were performed. This was presumably due to some bacterial cells striking the filter surface perpendicularly and, thus, passing through it, since the transverse diameter of parent and minicells is the same, being 400 nm. To eliminate residual bacterial cells, we took advantage of the fact that under stress-inducing conditions, such as growth in high salt, septum formation is incomplete during bacterial cell division, resulting in filament formation (Mattick et al., 2000). As shown in Figure 1C, incubation in the presence of 5% NaCl for 4 hr reliably converted parent bacteria into filaments of various lengths. This step was thus incorporated after the initial 0.45 μm crossflow filtration steps and the resulting filtrate was subjected to 0.2 μm crossflow filtration to remove small contaminants like bacterial membrane blebs, intracellular components, cellular debris, free nucleic acids, and endotoxin. These pass through the 0.2 μm filter, but minicells and residual bacterial cells are retained. The retentate was then filtered through a 0.45 μm dead-end filter and both the filtrate and retentate were subjected to FACS analysis. This revealed that filaments were only present in the retentate and, thus, were entirely eliminated from the filtrate. As a result, the final minicell preparation was sterile as confirmed by plating the entire preparation on growth agar plates and incubating it overnight at 37°C to demonstrate the absence of bacterial colonies. Additionally, preparations were grown for 14 days in thioglycolate broth to demonstrate the absence of any slow-growing organisms. Minicells were enumerated by FACS analysis, with a yield of approximately 5×10^{10} to 10^{11} minicells (Figure 1D) from a 6 L starting culture being routinely obtained. We also demonstrated that minicells can be lyophilized in a cryoprotectant and stored for at least 4 months (the longest period tested) and then successfully reconstituted (data not shown).

Efficient Packaging of Chemotherapeutic Drugs into Minicells, Drug Quantitation, and Targeting Using Bispecific Antibodies

To determine if minicells can be packaged with chemotherapeutic drugs down a concentration gradient despite an intact bilayer membrane, preparations of purified minicells (10^9) derived from *S.* Typhimurium and *E. coli* *min*CDE− mutants were separately incubated with the chemotherapeutic drugs, doxorubicin (Dox; 60 μg/ml), Oregon Green 488-conjugated paclitaxel (Pac; 100 μg/ml), and BODIPY FL-conjugated vinblastine (Vin; 100 μg/ml). Minicell drug loading was evident with all drugs, either by the red autofluorescence of Dox (Figure 1Ea) or green fluorescence of the minicells packaged with vinblastine or paclitaxel (Figures 1Eb and 1Ec). Targeting of minicells was achieved using bispecific antibodies (BsAb), in which one arm recognizes the O-antigen component of the minicell surface LPS and the other, a cell-surface receptor specific for the mammalian cell to be targeted, for example, EGFR (El-Rayes and LoRusso, 2004) or HER2/*neu* receptor (Slamon et al., 1987) on breast and ovarian cancer cells, respectively. Linkage of these two antibodies via their Fc regions was achieved by the use of protein A/G. Drug loading and BsAb linkage were confirmed as shown in Figures 1E and 1F. Drug-packaged and targeted minicells were designated ^{EGFR}minicells$_{Dox}$, for example, for those packaged with Dox and targeted using an anti-EGFR BsAb, or ^{HER2}minicells$_{Pac}$, for those packaged with Pac and targeted using an anti-HER2 BsAb. In additional studies, we found that minicells could also be packaged with other chemotherapeutic drugs, including carboplatin, cisplatin 5-fluorouracil (5-FU), gemcitabine, irinotecan, and kinesin spindle protein inhibitor monastrol. To determine the kinetics of minicell drug packaging, the amount of drug packaged per minicell in response to varying concentrations of drug in the incubation solution or varying times of incubation were evaluated. As shown in Figure 2A, drug packaging was dependent on, and directly

the red autofluorescing Dox within the minicell (Fb). In (Fc), minicells packaged with Oregon Green 488-conjugated Fluoro-Pac (green fluorescence) were coated with Alexa Fluor 594-conjugated BsAb (red fluorescence). The intense yellow fluorescence shown is due to the overlay of the red surface (BsAb) and green cytoplasm (Pac). Scale bar, 1 μm.

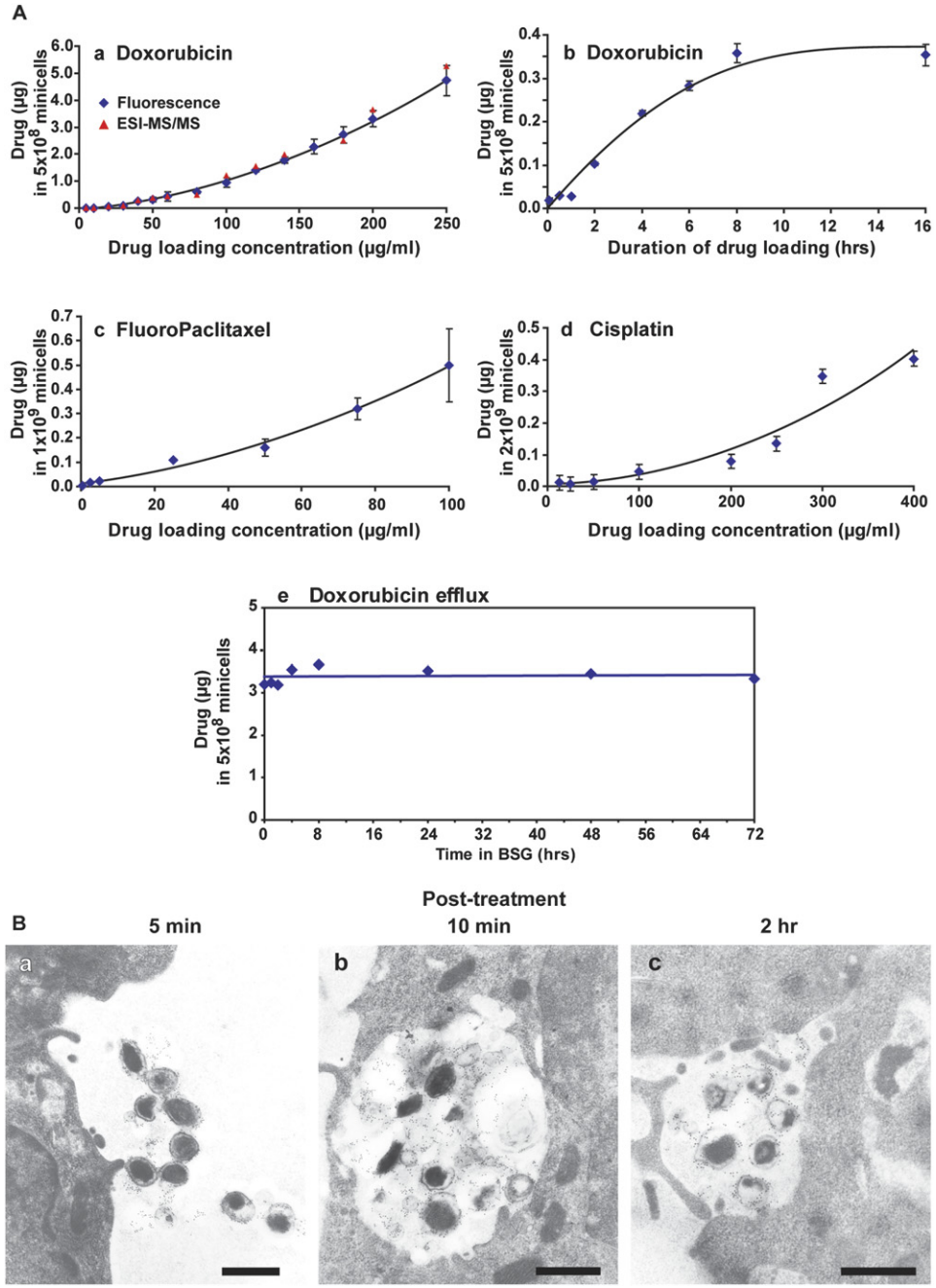

Figure 2. Drug Quantitation in Minicells, Drug Efflux, and Intracellular Breakdown of Minicells

(A) Quantitation of minicell loading when incubated in the presence of different drug concentrations (Aa, Ac, and Ad) and for different times (Ab). In (Aa, Ac, and Ad), minicells were incubated for 1 hr with different concentrations of Dox, Pac, or cisplatin. Drug loading was determined after extraction from minicells and quantitation by HPLC and fluorescence detection or LC-MS/MS. In (Ab), minicells were incubated with Dox (60 μg/ml) for the times shown (n = 6). To evaluate drug efflux after loading, minicells were incubated in an external concentration of Dox (200 μg/ml). The minicells$_{Dox}$ were incubated in BSG for 72 hr at 4°C and Dox was extracted and quantitated from samples (triplicate) at the time points shown (Ae). Despite prolonged incubation in BSG no drug efflux was observed. Error bars, ± SEM.

(B) Phagocytic uptake of nontargeted minicells by macrophages. *S.* Typhimurium-derived minicells were incubated with mouse macrophage cells (RWA 264.7) at a ratio of 100:1. At the times indicated, the cells were subjected to immunogold labeling using anti-O-antigen primary, and gold (10 nm)-conjugated anti-mouse secondary antibody followed by TEM. Immunogold-labeled minicells are evident on the macrophage cell surface (Ba). At later times numerous minicells can be seen within intracellular vacuoles (Bb and Bc) where disruption of their cell walls is evident. Scale bar, 500 nm.

related to, both the drug concentration in the incubation solution (Figures 2Aa, 2Ac, and 2Ad), and the time of incubation (Figure 2Ab). With the incubation of 5×10^8 minicells for 1 hr with 250 μg/ml Dox, 100 μg/ml Pac, or 400 μg/ml cisplatin, the amount packaged was ~4.8 μg, 0.25 μg, and 0.1 μg, respectively. This equates to ~10 million, 220,000, and 614,000 drug molecules packaged per minicell, respectively. To examine drug efflux, $minicells_{Dox}$ were incubated for up to 72 hr in buffered saline gelatin (BSG) before drug extraction and quantitation. This confirmed a lack of drug efflux (Figure 2Ae). These findings therefore show that minicells can be readily packaged with chemotherapeutic drugs, whether they be hydrophilic (irinotecan), hydrophobic (Pac, cisplatin, carboplatin, monastrol), or amphipathic (Dox, vinblastine, 5-FU), and that diffusion across the minicell phospholipid bilayer-membrane is essentially unidirectional; efflux not being observed even with extensive minicell washing and incubation in drug-free solution.

Intracellular Processing of Minicells and Targeted Minicell-Mediated Drug Delivery to Cancer Cells In Vitro

Following internalization, TEM studies of minicell-treated cancer cells and mouse macrophage cells showed that the minicells were localized in intracellular vacuoles (Figure 2B). As many as five to eight minicells were localized in a single vacuole, with a single cell carrying as many as 40 to 50 minicells. At later time points, minicell integrity was lost and membrane fragments carrying LPS were evident within vacuoles, indicating minicell breakdown (Figure 2Bc).

To determine if BsAb-targeted, drug-packaged minicells can deliver bioactive drug intracellularly into human cancer cells, we incubated MDA-MB-468 human breast adenocarcinoma cells with $^{EGFR}minicells_{Dox}$ (10^9), and monitored their fate over 48 hr by confocal microscopy. As controls, $^{CMV}minicells_{Dox}$ where the BsAb is directed to an irrelevant antigen, CMV (cytomegalovirus capsid protein), and non-Dox-packaged ^{EGFR}minicells, were also studied.

As shown in Figure 3A, within 4 hr, only MDA cells treated with $^{EGFR}minicells_{Dox}$ and ^{EGFR}minicells showed large numbers of minicells intracellularly (green fluorescence due to BsAb attached to the minicell surface; Figures 3Ab and 3Am). Since the nontargeted minicells and $^{CMV}minicells_{Dox}$ did not adhere to the MDA cell surface and were not internalized (absence of green or red fluorescence; Figure 3Ak), it is likely that the BsAb-targeted $^{EGFR}minicells_{Dox}$ and ^{EGFR}minicells gained entry into the MDA cell cytoplasm via EGFR-mediated endocytosis. At 4 hr, the minicells were confined to the MDA cell cytoplasm since the overlaid image (Figure 3Ae) showed that the nucleus remained blue, similar to the DAPI-stained nucleus seen in Figure 3Ad. Additionally, in the overlaid image (Figure 3Ae), colocalization of the minicell- and Dox-associated green and red fluorescence, respectively, showed yellow fluorescence in the MDA cell cytoplasm suggesting that the drug had not yet been released from the minicells. In contrast, by 16 hr to 24 hr, the MDA nucleus showed intense diffuse red fluorescence (Figure 3Ah; compare with Figure 3Ac) and the minicell-associated green fluorescence had significantly decreased (compare Figures 3Ab and 3Ag) only in the $^{EGFR}minicells_{Dox}$-treated cells. Nuclear presence of Dox was confirmed in the overlaid images, which showed violet fluorescence (Figure 3Aj) due to colocalization of the blue DAPI stain (Figure 3Ai) and red Dox fluorescence (Figure 3Ah), while all other overlaid images showed only the blue fluorescence of DAPI (Figures 3Al and 3An). This suggested that the Dox had now been released from the minicell cytoplasm and had translocated to the nucleus. By 48 hr, gross abnormalities in cellular integrity, nuclear disorganization, and cell death were readily apparent (Figure 3Ao), presumably due to the cytotoxic effect of Dox within the nucleus. In contrast, minicell attachment to MDA cells was not observed at 4 or 24 hr with $^{CMV}minicells_{Dox}$ (Figures 3Ak–3Al; note the lack of green or red fluorescence), whereas attachment but not Dox was observed with ^{EGFR}minicells (Figures 3Am and 3An; note perinuclear green fluorescence, but lack of red or violet fluorescence). With both these controls, cell integrity was unaltered, even at 48 hr (data not shown). Specificity of receptor attachment via BsAb-targeted minicells was evaluated by coincubating MDA cells with specifically (^{EGFR}minicells) and nonspecifically (^{CD33}minicells) targeted minicells where the BsAbs were conjugated to Alexa Fluor 488 fluorescent dye. Only the ^{EGFR}minicells specifically adhered (>95%) to MDA cells (Figure 3B). Cytotoxicity of minicell-delivered Dox was also apparent when cell viability was evaluated quantitatively using the colorimetric MTT assay (Cory et al., 1991). Cell death was similar for MDA cells incubated with $^{EGFR}minicells_{Dox}$ or free Dox, whereas viability remained largely unchanged when cells were treated with nontargeted $minicells_{Dox}$ (Figure 3C).

BsAb-Targeted, Minicell-Mediated Chemotherapeutic Drug Delivery to Human Breast, Leukemia, and Ovarian Cancer Cell Xenografts In Vivo

We next investigated if receptor-targeted, drug-packaged minicells could deliver Dox to human cancer xenografts in vivo. As shown in Figure 4A, compared to control groups that received intravenous (i.v.) or intratumoral (i.t.) nontargeted $minicells_{Dox,}$ or BsAb (anti-O antigen/anti-EGFR) plus free Dox, administration of $^{EGFR}minicells_{Dox}$ to mice with MDA xenografts (tumor volume ~50–70 mm^3) resulted in highly significant inhibition of tumor growth. Failure to see tumor growth inhibition with $minicells_{Dox}$ indicates that BsAb-mediated targeting is essential. Importantly, tumor regression was readily apparent when animals with very large tumors (~800–1000 mm^3), which had developed following treatment with nontargeted $minicells_{Dox}$ for 7 weeks (Figure 4A, day 63), were switched to treatment with $^{EGFR}minicells_{Dox}$. This resulted in a dramatic reduction in tumor volume to ~100–150 mm^3 after only 6 days (Figure 4A, day 79), which was maintained for the

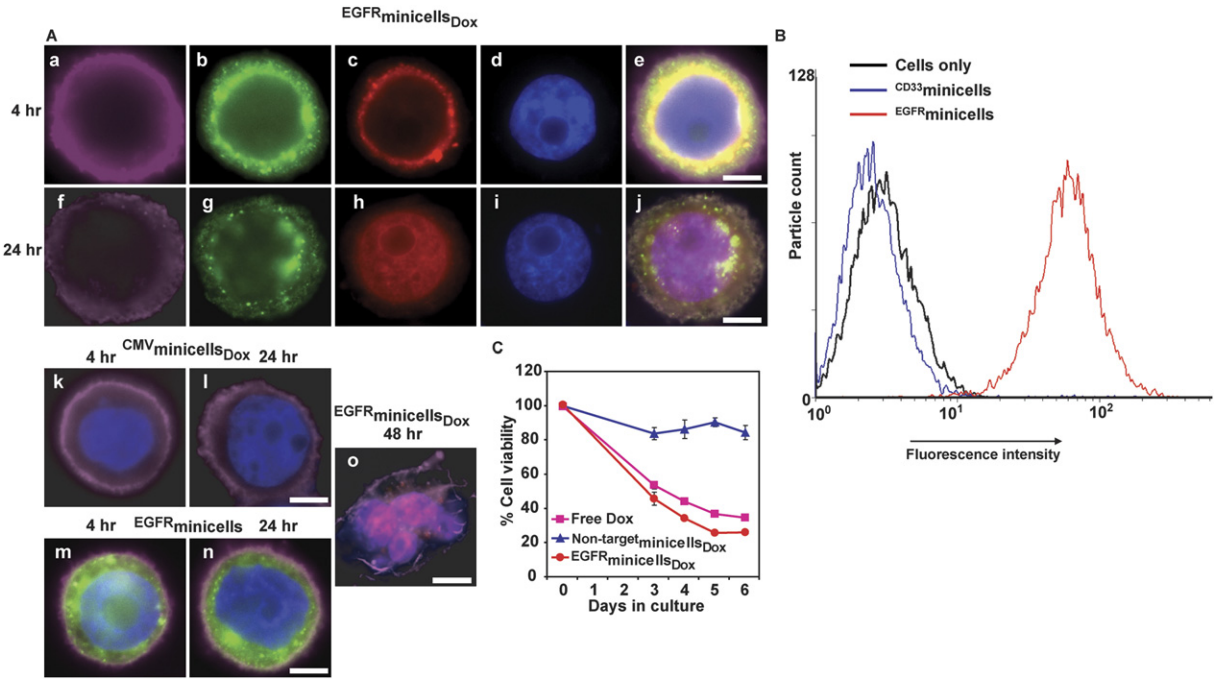

Figure 3. Dynamics of Minicell Attachment, Endocytosis, Breakdown and Drug Delivery, and Cytotoxicity

(A) MDA-MB-468 cells were treated with ^{EGFR}minicells$_{Dox}$, ^{EGFR}minicells, or ^{CMV}minicells$_{Dox}$ and visualized by confocal microscopy over 48 hr. MDA cell membrane was visualized with Alexa Fluor 647-conjugated anti-EGFR mAb (violet fluorescence), minicells by Alexa Fluor 488-conjugated anti-O antigen/anti-EGFR or /anti-CMV BsAbs (green fluorescence) attached to their surface, Dox by its red autofluorescence, and MDA nuclei by DAPI staining (blue fluorescence). The images shown are for MDA cells treated with ^{EGFR}minicells$_{Dox}$ (4 hr, Aa–Ae; 24 hr, Af–Aj; 48 hr, Ao), ^{CMV}minicells$_{Dox}$ (4 hr, Ak; 24 hr, Al), and ^{EGFR}minicells (4 hr, Am; 24 hr, An). Overlaid images for ^{EGFR}minicells$_{Dox}$ include, (Ae), a composite of Aa to Ad, and (Aj), a composite of Af to Ai. The ^{CMV}minicells$_{Dox}$ and ^{EGFR}minicells images are composites corresponding to those for ^{EGFR}minicells$_{Dox}$ (Ae and Aj), except that the individual images showing EGFR-, BsAb-, Dox-, and DAPI-fluorescence are not shown. Only ^{EGFR}minicells$_{Dox}$ and ^{EGFR}minicells specifically attached and internalized in MDA cells (Ab, Am). Postinternalization, the minicells are broken down to release Dox, which is translocated to the nucleus (Ah, Aj). After 48 hr, loss of cellular and nuclear integrity is seen (Ao). Scale bar, 20 μm.

(B) FACS analysis of MDA cells incubated for 30 min with specifically targeted ^{EGFR}minicells or nonspecifically targeted ^{CD33}minicells. The anti-EGFR and CD33 BsAbs were labeled with Alexa Fluor 488 (Molecular Probes) and the result showed that greater than 99% of the cells fluoresced only when coincubated with ^{EGFR}minicells.

(C) Cytotoxicity of Dox delivered to MDA cells by ^{EGFR}minicells$_{Dox}$ was evaluated by incubating cells (10^7) with either free Dox (50 ng/ml), 10^9 minicells$_{Dox}$, or ^{EGFR}minicells$_{Dox}$, (10^9 minicells contained ~900 ng Dox) and then monitored for viability. Error bars, ± SEM.

rest of the study. An additional beneficial effect of Dox delivery via targeted minicells is the markedly smaller amounts of drug required to affect tumor growth inhibition/regression with minicell-packaged delivery versus free drug administration. Thus, even ~1875 times the amount of free Dox (150 μg) versus minicell-packaged Dox (0.08 μg) did not produce comparable xenograft growth inhibition (see for example Figure 4A, day 63, G2, G3, or G4 versus G7 or G8). Finally, phlebitis, thought to result from extravasation of drug and leading to local site vesicant/tissue damage, a well-recognized complication of i.v. Dox (Ewesuedo and Ratain, 2003) and one that was clearly evident in animals treated here with free drug (Figure 4E), was not observed in any of the mice treated with minicells$_{Dox}$.

We investigated if a hydrophobic drug like Pac could also be delivered effectively to mice with MDA xenografts by repeating the studies shown in Figure 4A, except using ^{EGFR}minicells$_{Pac}$ as the experimental treatment. Similar highly significant inhibition of tumor growth (Figure 4B, $p < 0.0003$ and $p < 0.0006$ for the G7 and G8 groups versus all others, respectively) was evident both in mice treated i.v. or i.t. with ^{EGFR}minicells$_{Pac}$. This was despite an ~8000-fold lower Pac dose being administered via ^{EGFR}minicells$_{Pac}$ (~0.05 μg/mouse) compared to free Pac (~400 μg/mouse). Moreover, none of the mice treated with either ^{EGFR}minicells$_{Dox}$ or ^{EGFR}minicells$_{Pac}$ showed signs of toxicity, such as weight loss, fever, lethargy, loss of appetite, or death.

To investigate if specific targeting of tumor cells via BsAb-coated, drug-packaged minicells was essential for the observed antitumor effects, xenografts were established using A549 lung carcinoma cells that overexpress EGFR (~448,000/cell) but not the plasma membrane marker, CD33 (Figure 4C). These mice were given a range of control treatments (Figure 4D; G1 to G10 mice) and two experimental treatments with ^{EGFR}minicells$_{Pac}$ (G11) and ^{CD33}minicells$_{Pac}$ (G12). Consistent with an essential role of the targeting BsAb, ^{CD33}minicells$_{Pac}$ had no antitumor effect, whereas ^{EGFR}minicells$_{Pac}$ were highly effective in

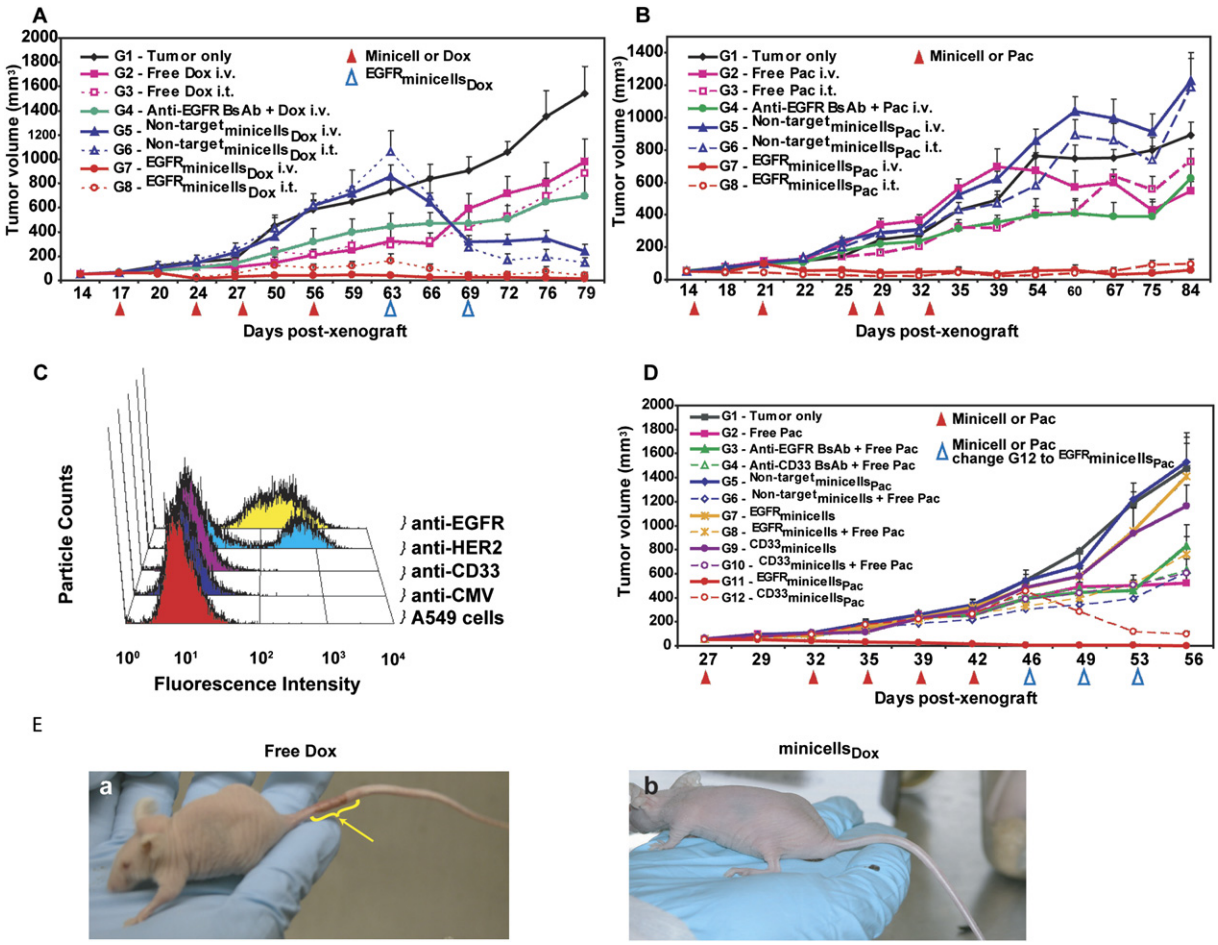

Figure 4. Tumor Xenograft Treatments with BsAb-Targeted, Dox- or Pac-Packaged Minicells, and Safety in Mice

Inhibition/regression of tumor growth in mice with MDA-MB-468 xenografts via EGFR- or CD33-targeted, Pac- or Dox-packaged minicells, demonstration that BsAb-mediated targeting of minicells to tumor cells is necessary for antitumor effects and safety of minicell-delivered Dox. Error bars for all graphs, ± SEM.

(A) Mice (n = 11/group) bearing MDA xenografts were treated i.v. or i.t. with either free Dox (7.5 μg/gm, ~150 μg/mouse) or BsAb (anti-O-antigen/anti-EGFR) plus free Dox (7.5 μg/gm, i.v. only), minicells$_{Dox}$ (10^8), or ^{EGFR}minicells$_{Dox}$ (10^8); the Dox-packaged minicells carrying 0.08 μg Dox per dose. Inhibition of tumor growth is evident by day 56 with ^{EGFR}minicells$_{Dox}$ ($p < 0.0004$ for tumor volume versus all other treatments), but not with the other treatments. At day 63, the groups treated with nontargeted minicells$_{Dox}$ were switched to ^{EGFR}minicells$_{Dox}$ treatment (open blue triangles). This resulted in rapid and highly significant tumor regression ($p < 0.001$ for tumor volume at day 69 versus day 63).

(B) The studies were performed as detailed in Figure 4A, except that the animals were given either minicells packaged with Pac (0.05 μg/dose) or free Pac (20 μg/gm, ~400 μg/mouse). Inhibition of tumor growth is evident by day 25 in the groups receiving ^{EGFR}minicells$_{Pac}$ ($p < 0.0004$ for tumor volume versus all other treatments), but not in the other groups.

(C) Receptor quantitation study on A549 lung carcinoma cell line where EGFR, HER-2/*neu*, and CD33 were quantitated. As negative controls, anti-CMV MAb was used along with untreated cells. Cells were treated with the various primary antibodies and a Phycoerythrin (PE)-labeled secondary antibody followed by FACS analysis. Receptor quantitation was carried out using the Quantum PE MESF kit (Molecules of Equivalent Soluble Fluorochrome; Bang Labs). Mean receptor numbers were EGFR (~447,515) and HER2 (~1686 for 50% cells and ~917,352 for the remaining 50%). The cells did not stain for CD33 or CMV.

(D) A549 xenograft with a range of different controls including free Pac (G2), specifically and nonspecifically targeted BsAbs followed by free Pac (G3 and G4), nontargeted, Pac-packaged minicells (G5), nontargeted minicells followed by free Pac (G6), EGFR-targeted minicells (G7) and followed by free Pac (G8), nonspecifically targeted minicells (G9) and followed by free Pac (G10) as shown in the figure. The experimental groups consisted of ^{EGFR}minicells$_{Pac}$ (G11; A549 overexpresses EGFR) and ^{CD33}minicells$_{Pac}$ (G12; A549 does not express CD33). Inhibition of tumor growth was evident in G11 mice and not in any other group including G12. On day 42, when the tumor volume was ~400–500 mm^3, the treatment of G12 mice was changed to ^{EGFR}minicells$_{Pac}$ which resulted in rapid tumor regression ($p < 0.0003$ at day 56 between G12 versus all groups).

(E) Safety of minicell-packaged i.v. Dox delivery. Mice given free Dox injected i.v. into the tail vein developed severe phlebitis (a; arrow and bracketed region of the tail). However, i.v. minicells$_{Dox}$ and ^{EGFR}minicells$_{Dox}$ were well tolerated in all animals, without inflammatory reaction (b).

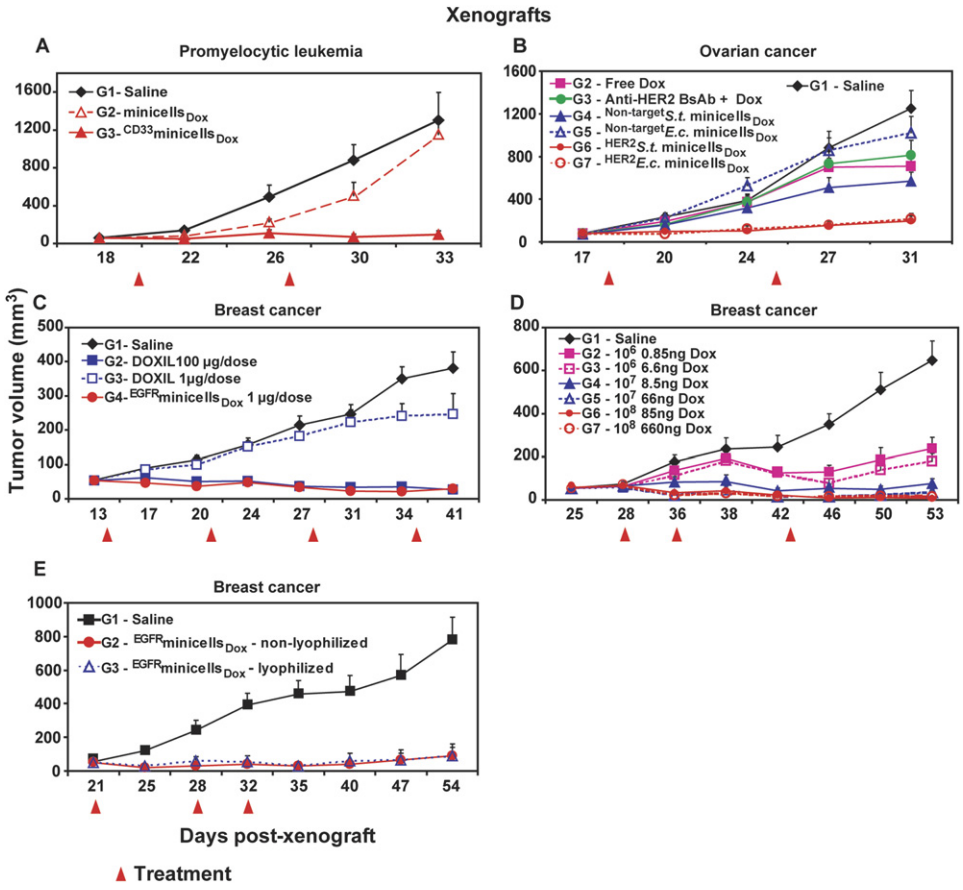

Figure 5. Antitumor Effects in Tumor Xenografts, Dose Response, and Stability

Antitumor effects via *S*. Typhimurium or *E. coli*-derived ^{HER2}minicells$_{Dox}$, comparison of minicells$_{Dox}$ versus liposomal$_{Dox}$, minicells$_{Dox}$ dose response, minicells$_{Dox}$ stability following lyophilization and antitumor effects in promyelocytic leukemia cell xenografts following ^{CD33}minicells$_{Dox}$ treatment. Error bars for all graphs, ± SEM. All xenografts have 11 mice per group. Arrowheads below the abscissae indicate the days that minicell treatments were given.

(A) Mice with HL-60 promyelocytic leukemia cell xenografts were treated i.v. with 5 × 10^8 ^{CD33}minicells$_{Dox}$ carrying 1 μg Dox/dose. Minicells$_{Dox}$ were used as controls. Inhibition of tumor growth was evident by day 33 for animals treated with ^{CD33}minicells$_{Dox}$ ($p < 0.0001$ for tumor volume in G3 mice versus all controls).

(B) Inhibition of tumor growth in mice with SKOV3 ovarian cancer cell xenografts treated with Dox-packaged minicells derived from *S*. Typhimurium or *E. coli* and targeted to the HER2 receptor. Mice with SKOV3 xenografts were treated i.v. with either free Dox (7.5 μg/gm; ~150 μg/mouse), BsAb (anti-O-antigen/anti-HER2/*neu*) plus free Dox (7.5 μg/gm, i.v. only), minicells$_{Dox}$ (10^8), or ^{HER2}minicells$_{Dox}$ (10^8); the minicells carrying 0.08 μg Dox per dose. Inhibition of tumor growth is evident by day 24 for animals treated with ^{HER2}minicells$_{Dox}$ derived from either *S*. Typhimurium or *E. coli* ($p < 0.0009$ and < 0.0014 for tumor volume versus all controls respectively).

(C) Comparison of liposomal-Dox (DOXIL) and ^{EGFR}minicells$_{Dox}$ treatment of mice with MDA xenografts. G2 mice received a high dose of DOXIL (100 μg dox/dose) while G3 mice received DOXIL in a dose that provided the same amount of Dox (1 μg) as the G4 mice that were treated with ^{EGFR}minicells$_{Dox}$. Highly significant tumor growth inhibition ($p < 0.0001$) was achieved in G2 and G4 mice, but not in G3.

(D) Dose-related effects of i.v. ^{EGFR}minicells$_{Dox}$ on tumor growth. Mice with MDA xenografts were treated with 10^6, 10^7, or 10^8 doses of ^{EGFR}minicells$_{Dox}$; each minicell dose carrying the amount of Dox indicated. Note that tumor volumes in all treated groups are significantly less by day 42 ($p < 0.001$) than in the untreated (tumor only) control animals.

(E) Stability of the drug-packaged and BsAb-targeted minicells. Mice with MDA xenografts were treated with either freshly prepared or lyophilized and reconstituted ^{EGFR}minicells$_{Dox}$. Both treatment groups (G2 and G3) showed similar significant degrees of tumor growth inhibition compared to the control group (G1), by day 25 ($p < 0.0001$).

tumor stabilization. This was further confirmed when G12 mice treated with ^{CD33}minicells$_{Pac}$ were switched to treatment with ^{EGFR}minicells$_{Pac}$ on day 46 when their tumors were ~400–500 mm^3. This resulted in rapid tumor regression.

Since it is possible that anti-EGFR and anti-HER2/*neu* antibodies may elicit antiangiogenic effects (Petit et al., 1997; Izumi et al., 2002), we carried out an HL-60 promyelocytic leukemia cell xenograft study in which minicells$_{Dox}$ were targeted to an HL-60 cell-surface marker CD33. Antibodies to this cell-surface marker are not known to exhibit antiangiogenic effects. Highly significant tumor growth inhibition was also observed in these mice (Figure 5A), suggesting that suppression of tumor growth

by targeted, drug-packaged minicells is not dependent on antiangiogenic mechanisms. However, further work will be required to rule out the possibility that EGFR and HER2-targeted minicells have both direct and antiangiogenic effects. We also investigated if drug-packaged minicells could be used to treat SKOV3 ovarian cancer xenografts targeted via their overexpressed HER2/*neu* receptor. Additionally, in these studies minicells derived from both *S*. Typhimurium and *E. coli minCDE*− strains were tested for efficacy of drug delivery. The experimental groups received ^{HER2}minicells$_{Dox}$, and again, significant antitumor effect was seen in mice treated with either *S*. Typhimurium- or *E. coli*-derived ^{HER2}minicells$_{Dox}$ (Figure 5B).

Comparison with Liposomal-Dox, Dose Response, and Minicell Stability

We compared the antitumor activity of liposomal-Dox (DOXIL) with that of ^{EGFR}minicells$_{Dox}$. Mice with MDA xenografts were treated i.v. with DOXIL carrying high (100 μg) or low (1 μg) doses of Dox; the latter being the dose also given to animals treated with ^{EGFR}minicells$_{Dox}$. Only the dose of DOXIL providing a 100-fold higher amount of Dox produced the same degree of tumor growth-inhibition as that seen with the ^{EGFR}minicells$_{Dox}$ treatment that provided only 1 μg of Dox (Figure 5C).

We also investigated the dose of targeted, drug-packaged minicells required to achieve a significant antitumor effect, using 10^6, 10^7, and 10^8 ^{EGFR}minicells$_{Dox}$, each packaged with two different amounts of Dox and given i.v. to mice with MDA xenografts. Figure 5D shows that a dose of 10^8 ^{EGFR}minicells$_{Dox}$ was most effective in achieving tumor growth inhibition, whether carrying 85 ng or 660 ng of drug. The 10^7 and 10^6 doses of $^{>EGFR}$minicells$_{Dox}$ were also effective, with the former being more effective than the latter. Thus, there is a clear relationship between minicell dose and antitumor efficacy. To determine the stability of the complete therapeutic entity, ^{EGFR}minicells$_{Dox}$ were lyophilized in an iso-osmotic cryoprotectant, trehalose, reconstituted in sterile physiological saline and injected i.v. into mice with MDA xenografts. Another group of mice were given freshly prepared ^{EGFR}minicells$_{Dox}$. Both preparations were shown to be equally effective in stabilizing tumor growth (Figure 5E).

Minicell Biodistribution in Mice, Case Studies in NHL Dogs, and Minicell Safety in Pigs

The biodistribution of i.v.-administered minicells bearing ^{125}I-labeled BsAbs was studied in nude mice with MDA xenografts that overexpress EGFR. These studies revealed that at 2 hr posttreatment, ~30% of the ^{EGFR}minicells were localized in the tumor, as compared to only ~1.3% of nonspecifically targeted ^{CMV}minicells (Figure 6Aa). In addition, in animals given radioiodinated BsAb alone (^{EGFR}BsAb or ^{CMV}BsAb), only ~3 and 2.2%, respectively, of the radiolabel was localized in the tumor at 2 hr. By 6 (Figure 6Ab) and 24 hr (Figure 6Ac), ~4.6% and ~0.5%, respectively, of specifically targeted ^{EGFR}minicells remained in the tumors. These data suggest that in contrast to nonspecifically targeted ^{CMV}minicells, ^{EGFR}minicells are not only localized but are concentrated in the tumor microenvironment. This likely results from rapid extravasation of ^{EGFR}minicells from the circulation via the leaky vasculature of the tumor (passive targeting), followed by engagement of tumor cell-surface EGFRs (active targeting), adherence, and endocytosis. While nonspecifically targeted ^{CMV}minicells may also rapidly extravasate from the circulation, they are not retained in the tumors as they are unable to target EGFRs and are washed out after tumor isolation and extensive saline washing of the tissue.

Biodistribution of minicell-packaged drug was determined following i.v. administration of ^{EGFR}minicells$_{Dox}$, nontargeted minicells$_{Dox}$, or free Dox to nude mice with MDA xenografts (tumor volume between 140 and 170 mm^3). As shown in Figure 6B, at 6 hr, ~30% of the Dox dose administered by the ^{EGFR}minicells$_{Dox}$ was found in the tumors, as compared to only ~1% of free Dox and ~0.34% of that in minicells$_{Dox}$. Moreover, similar results were observed in animals with much larger tumors (400–600 mm^3), in which ~28.1% of the Dox dose in ^{EGFR}minicells$_{Dox}$ was found in the tumors at 6 hr, as compared to only ~0.21% of that in nontargeted, minicells$_{Dox}$, and ~1.8% for free Dox. Plasma concentration of Dox at both time points was undetectable. Thus, targeted minicell delivery provides at least a 30-fold enrichment in tumor drug delivery. At 6 hr, biodistribution to the liver and spleen was higher with the ^{EGFR}minicells$_{Dox}$ and minicells$_{Dox}$ compared to free Dox and showed a slow decrease by 24 hr. At 6 hr, the biodistribution to the lungs was also found to be higher with ^{EGFR}minicells$_{Dox}$ administration. However, it was rapidly cleared from this tissue, as was evident by the marked fall in lung Dox-levels at 24 hr. At 2 hr, minicell uptake in the liver (Figure 6Aa) for ^{EGFR}minicells and ^{CMV}minicells was not significantly different ($p = 0.095$), suggesting that both types of minicells accumulate in the liver at similar levels. The data are further confirmed in Figure 6B where the Dox concentration in the liver at 6 hr and 24 hr post-i.v. administration of minicells$_{Dox}$ or ^{EGFR}minicells$_{Dox}$ is similar.

The biodistribution studies reveal early localization of the minicells in the tumor and rapid clearance from all sites within 24 hr. These results are similar to other observations with noncoated nanoparticles (Jun et al., 2005) and is likely to be due to the passive targeting via the enhanced permeation and retention effect of the tumor-associated leaky vasculature.

The anticancer efficacy of the minicells was evaluated in two case studies in which dogs with advanced (stage 4) T cell non-Hodgkin's lymphoma (NHL) were treated i.v. with $^{anti\text{-}canine\text{-}CD3}$minicells$_{Dox}$. One dog (4 kg) received a total of five doses over 35 days, and the other dog (40 kg) received seven doses over 48 days providing total amounts of Dox of 24 μg and 584 μg, respectively. Both dogs demonstrated marked tumor regression, as evident by highly significant reductions in lymph node size (Figure 7A), with the smaller dog also developing tumor lysis syndrome (hyperkalemia) by day 37 (data not shown). The proinflammatory cytokines, TNFα (Figure 7B) and IL-6

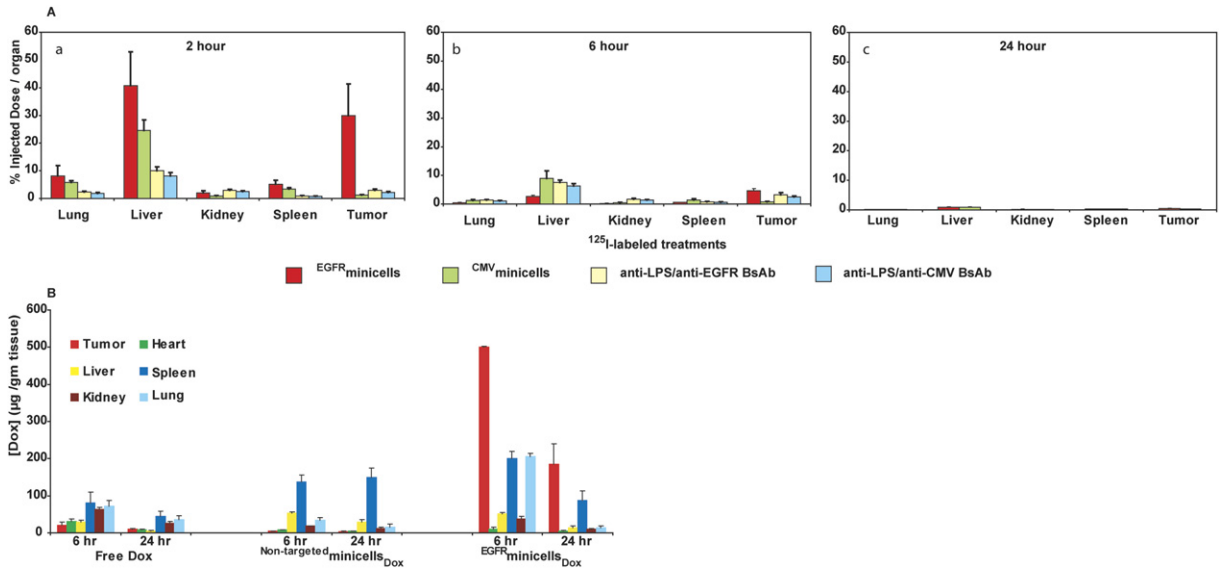

Figure 6. Biodistribution of ^{125}I-Labeled Minicells and Dox Delivered via ^{EGFR}minicells$_{Dox}$ in Nude Mice Bearing Breast Cancer Xenografts

Error bars for all graphs, ± SEM.

(A) Biodistribution of ^{EGFR}minicells and ^{CMV}minicells (~3.2 × 10^9 minicells per dose) bearing ^{125}I-labeled BsAbs determined following their i.v. administration to nude mice carrying MDA xenografts. Tumor, spleen, liver, kidney, and lung were excised from five mice per treatment at 2, 6, and 24 hr, and radioactivity was determined by γ spectroscopy. (Aa) At 2 hr posttreatment, ~30% of the ^{125}I-labeled ^{EGFR}minicells were localized in the tumor compared to only ~1.3% of the ^{125}I-labeled ^{CMV}minicells, ~3% of the ^{EGFR}BsAb, and ~2.2% of the ^{CMV}BsAb. (Ab and Ac) The various treatments were rapidly cleared from the tissues by 24 hr (Ab) and 48 hr (Ac).

(B) Biodistribution of Dox in vivo following i.v. administration of free dox (G1, 150 μg/dose), nontargeted minicells$_{Dox}$ (G2), ^{EGFR}minicells$_{Dox}$ (G3) to nude mice carrying MDA-MB-468 xenografts. Minicells (5 × 10^9/dose) carrying ~74 μg Dox were administered. Posttreatment, three mice from each group were euthanized at 6 hr and 24 hr. From each mouse, the tumor, spleen, liver, kidney, heart, and lung were excised and dox concentration was determined by HLPC and LC-MS/MS. At 6 hr ^{EGFR}minicells$_{Dox}$ delivered ~30% of the total Dox dose administered to the tumor compared to that delivered with free Dox (~1%) or minicells$_{Dox}$ (~0.34%).

(data not shown), did not increase in either dog despite repeated administration of ^{CD3}minicells$_{Dox}$. Surprisingly, anti-*S.* Typhimurium LPS titers also remained at background levels (Figure 7C), and evaluations of hematological indices, blood chemistries body weight, temperature, and urine analyses did not show any adverse changes with minicell administration (data not shown). The only mild potentially adverse response was a 0.5°C–1°C rise in temp postinjection. This was not sustained and had returned to normal by 4 hr postinjection.

We also evaluated the safety of i.v. administered minicells in three healthy pigs. Despite five successive i.v. doses of ~5 × 10^9 minicells, the pigs did not show adverse effects, as determined from evaluations of hematological indices and blood chemistries, as well as by assessment of respiratory rate, food intake, growth, the levels of proinflammatory mediators (TNFα, IL-6; Figures 7D–7E), and the acute phase reactant, haptoglobin (Figure 7F). Minor, variable increases in TNFα levels were observed at 1.5 hr after the administration of the third to fifth doses of minicells, which returned to baseline by 4–24 hr (Figure 7D). A weak serum anti-O antigen response was observed (Figure 7G) with the peak titer being evident after the second dose, which then decreased to even lower levels despite a further three doses. Postinjection, the pigs developed a minor fever but was not sustained and returned to normal within 2 hr.

DISCUSSION

We have developed a robust and versatile system for in vivo drug delivery using minicells, a bacterially-derived microreservoir-type carrier. These anucleate minicells (~400 nm diameter) can be readily produced in high yield from both Gram+ and Gram− organisms and purified free of parental bacteria, membrane blebs, nucleic acids, cellular debris, and free endotoxin, using commercially available filters. Minicells are stable and can be targeted to cancer cells in vitro and in vivo with high specificity and can, thus, be delivered in high concentration in vivo without toxicity. This was evident by the lack of a febrile response, weight loss, or skin/fur changes, etc. in the murine xenograft model, as well as by the lack of any abnormalities in blood chemistries (electrolytes, renal, and hepatic function) in pigs given repeated i.v. doses.

Minicells can package a range of anticancer chemotherapeutic drugs, such as doxorubicin, paclitaxel, irinotecan, 5-fluorouracil, cisplatin, carboplatin monastrol, and vinblastine despite their disparate structure, charge, hydrophobicity, and solubility. In contrast, attempts to

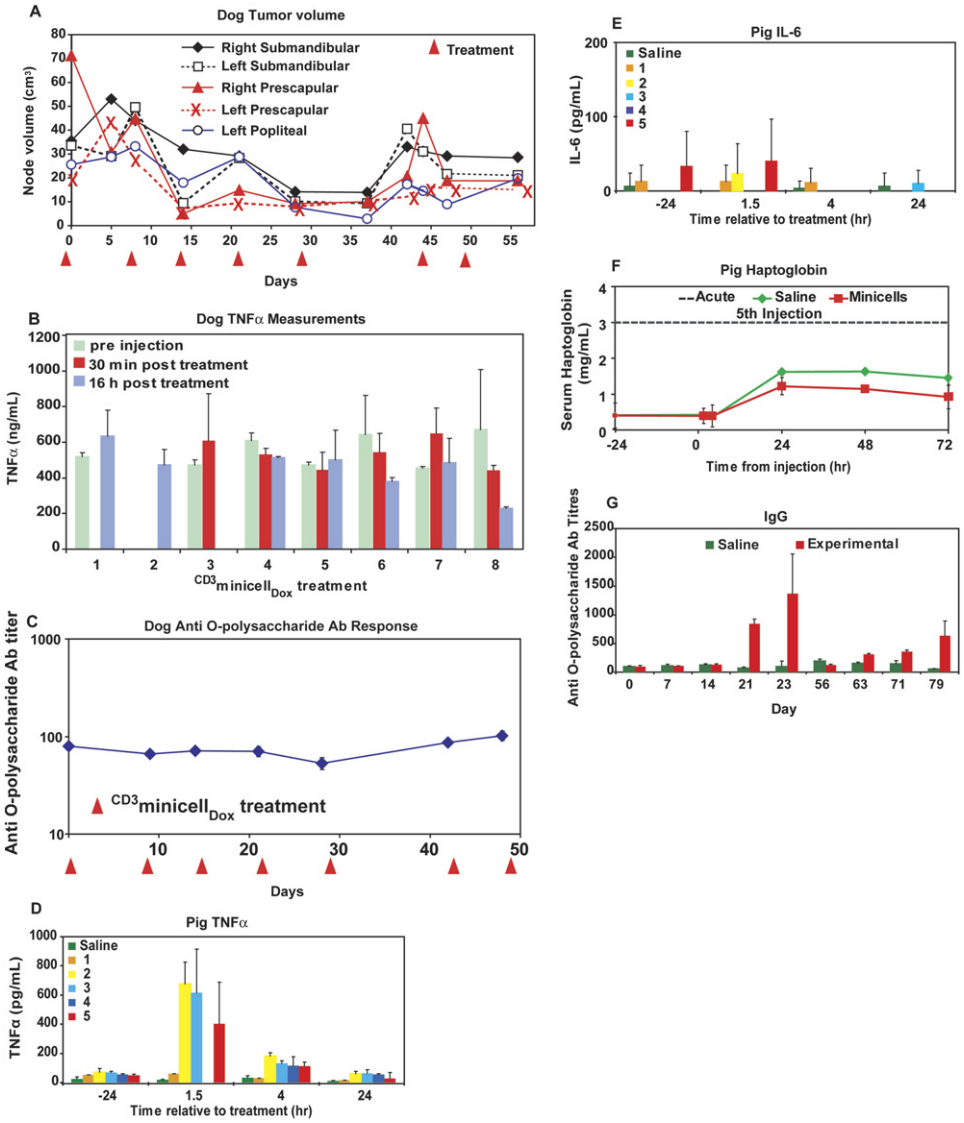

Figure 7. Antitumor Effects, Cytokine, Antibody Response in a Dog Suffering from NHL Treated with ^{CD3}minicells$_{Dox}$, and Safety of Minicells in Pigs

Error bars for all graphs; ± SEM.

(A) A dog (40 kg) with T cell NHL treated i.v. with Dox-packaged, canine CD3 T cell surface receptor-targeted minicells. Seven i.v. injections of ^{CD3}minicells$_{Dox}$ providing a total Dox dose of 584 μg were given. Tumor volume measurements of lymph nodes in the various areas indicated (determined as described in the Experimental Procedures) revealed significant regression as early as 15 days posttreatment ($p < 0.02$), which was highly significant by days 28 and 37 ($p < 0.0001$ and 0.0009, respectively). When the dog was left untreated between days 28 and 43, the nodes increased in size but again regressed with additional doses of ^{CD3}minicells$_{Dox}$ on days 43 and 48 ($p < 0.02$ versus the node sizes at day 43) suggesting that repeat dosing did not result in immune response-mediated exclusion of subsequent doses.

(B) Absence of TNFα response in the NHL dog in (A) treated with ^{CD3}minicells$_{Dox}$.

(C) Absence of an increase in anti-*S.* Typhimurium LPS titers in the NHL dog in (A) given seven repeat doses of ^{CD3}minicells$_{Dox}$. Note that the initial titer was determined before the first administration of ^{CD3}minicells$_{Dox}$.

(D–G) TNFα (D), IL-6 (E), serum haptoglobin ([F]; level at which acute phase reaction occurs in pigs is shown by a dotted line) and anti-*S.* Typhimurium O-antigen antibody (G) responses in healthy pigs given five repeat doses (doses 1 to 5 in each graph are color coded) of ~5×10^9 minicells.

package these drugs in other DDSs, such as liposomes, has required specific and significant alterations to either the drug or vector, resulting in compromised potency. The phenomenon of solute movement into bacterial cells and the extrusion of noxious solutes from bacterial cells has been studied for over 3 decades and is well understood. Drug loading of minicells is likely by diffusion down a concentration gradient with entry via nonspecific porin channels (Nikaido, 1996, 2003; Poole, 2002) in the outer membrane. Detailed studies of porins have revealed charged residues within the channels resulting in a transversal electric field that separates polar and nonpolar

solutes. Polar solutes are thought to be oriented in the field during permeation, which therefore becomes a fast one-dimensional diffusion process (Schulz, 1993). Nonspecific diffusion of hydrophobic solutes across the outer membrane is thought to occur through other channels such as the FadL family of outer membrane proteins (Van den Berg et al., 2004; Van den Berg, 2005).

We demonstrate that drug packaging in minicells is dependent on both the concentration of drug in the loading solution, and time of incubation (Figure 2A). The finding of smooth saturable loading kinetics is consistent with a normal or "Langmuir" isotherm, suggesting drug loading via a limited number of uptake sites (Denyer and Maillard, 2002). In addition to providing a barrier to solute entry, bacterial membranes contain a plethora of transport proteins involved in exporting solutes across their phospholipid bilayer membranes, against a concentration gradient (Piddock, 2006). Thus, retention of drug in minicells, after loading, is likely due to the metabolic inactivity that results from their lack of bacterial genome.

We also demonstrated that bispecific ligands, such as BsAbs, can be linked to the surface of minicells via the cell-surface-exposed O-polysaccharide component of LPS. This enables their specific targeting to cancer cell-surface receptors, such as EGFR, HER2/*neu*, CD33, and CD3. Linkage to O-polysaccharide via the BsAbs is extremely robust; a factor that likely accounts, in part, for the efficiency of this cell-targeting approach. In addition, adhesion of the BsAb/minicell complex to cell-surface receptors appears to trigger its rapid and efficient endocytosis, with subsequent minicell degradation and liberation of drug into the cytosol and nucleus, where it exerts its cytotoxic effect. As a consequence, targeted minicell-mediated drug delivery resulted in highly significant inhibition and even regression of tumor growth in vivo in mice with human breast, ovarian, leukemia, or lung cancer xenografts. Nonspecific activation of hematopoietic cells by bacterial products was not sufficient for antitumor effects since in each xenograft study, nontargeted or nonspecifically targeted minicells with or without packaged drug did not result in antitumor effects. Additionally, rapid tumor regression was evident in two dogs diagnosed with NHL when treated with ^{CD3}minicells$_{Dox}$. This versatility of targeting and of tumor growth inhibition, therefore, are additional, very favorable features of the minicell drug-delivery technology. Other approaches to make anticancer mAbs more effective include conjugation with cell-killing payloads such as anticancer drugs (Saleh et al., 2000; Sievers et al., 2001) to generate armed antibodies. However, there is a limitation of four to ten drug molecules that can be conjugated to an antibody. Our results reveal that an unprecedented 1 million to 10 million drug molecules can be packaged within a minicell.

Importantly, minicells were well tolerated with no adverse side effects or deaths in any of the actively-treated animals, despite repeat dosing. Given that the minicells are of bacterial origin, it is necessary to be cautious with parenteral administration since bacterial products are known to elicit potent inflammatory responses activated by Toll-like receptors (Shizuo and Takeda, 2004). We have therefore developed a robust minicell purification procedure to eliminate free endotoxin and free bacterial components. Interestingly, in the two dogs and three pigs studied, only the latter demonstrated a very short lived and mild TNFα response. This contrasts with TNFα levels as high as 20,000 pg/ml after i.v. injection of 2 μg/kg LPS in pigs (Myers et al., 2003). Interestingly, neither a TNFα response nor an increase in IL-6, another inflammatory cytokine, was observed in the tumor-bearing dogs despite repeat i.v. administration of high doses of minicells. Additionally, neither the pigs nor the dogs showed adverse effects in terms of their hematological indices, serum chemistries, food intake, or growth. Although our in vivo studies reveal weak immunogenicity of dominant minicell-surface exposed antigen, O-polysaccharide, and that repeat i.v. administration did not result in immune exclusion of subsequent doses, extensive evaluation of immunogenicity would be required to determine the nature of humoral and cellular immunity to the vehicle in both tumor-bearing and naive animals. Similarly, the safety data in pigs, although encouraging, must be considered preliminary and, prior to considering the minicell as a vector for human use, extensive toxicology, in vivo stability, etc. studies would be required. In recent times, excellent mouse models of human cancer have been developed and the above xenograft studies should be carried out in such models to provide greater insight regarding the potential and limitations of the minicell drug-delivery vector.

The most important feature of minicell drug delivery, however, is its ability to achieve inhibition/regression of tumor growth with delivery of amounts of drug that are markedly smaller than those required with systemic delivery of free drug. For example, with delivery of targeted minicells carrying Dox or Pac, tumor growth inhibition was significantly more marked in the xenograft models than with the administration of ~1875-fold and ~8000-fold higher amounts of their respective free drugs. Similarly, tumor lysis was observed in two NHL dogs despite receiving ~25,000-fold and 10,270-fold less Dox via minicell administration than that normally administered as part of conventional combination therapy. This remarkable efficacy may be due to the specificity of drug delivery directly into the target tumor cell. Although case studies in the two dogs is very encouraging, the data are anectodal and further dog clinical trial studies would be required. Biodistribution studies in tumor-bearing mice showed that within 6 hr post-i.v. administration of ^{EGFR}minicells$_{Dox}$, ~30% of the injected dose of Dox was found in the tumor, a result that is consistent with the rapid and highly significant antitumor effects seen in the mouse and dog studies. At this early time point, significant Dox concentration was also observed in the spleen, liver, and lungs and is likely to reflect the excess minicells being taken up by professional phagocytic cells that predominate in these organs of the reticuloendothelial system since Dox-associated toxicity was not observed in these organs in the mouse and dog studies.

Nano-sized DDSs, such as immunoliposomes, are currently believed to affect tumor targeting by an initial passive process involving extravasation from the leaky vasculature (pore sizes 200–1.2 μm; Hobbs et al., 1998; Yuan et al., 1994) that supports the tumor microenvironment. This is followed by active targeting via cancer cell-surface receptor engagement and endocytosis (Mamot et al., 2003). Although it has been shown that the abnormal tumor microenvironment is characterized by interstitial hypertension and that this phenomenon may limit access of anticancer antibody therapeutics, this does not appear to be an absolute barrier as is exemplified by immunoliposomes (Nielsen et al., 2002) and antibody conjugated to Quantum Dots (Gao et al., 2004). Similar considerations are likely to also underlie the antitumor efficacy of minicell-based drug delivery. Moreover, although not specifically evaluated, the ability to administer very small yet targeted doses of chemotherapeutics should allow the therapeutic potential of even highly toxic agents to be realized, and/or the use of complex combination or sequential therapy.

EXPERIMENTAL PROCEDURES

Reagents and Minicell Generation Purification, Enumeration, and Lyophilization

Detailed Supplemental Experimental Procedures (in the Supplemental Data available with this article online) describe bacterial strains, their growth, genomic DNA isolation, plasmids and oligonucleotides used (see Tables S1, S2, and S3) and their purification. Also detailed online include minicell generation by chromosomal deletion of the *min*CDE genes in parental bacteria and minicell purification to homogeneity, for example, free of contaminating parent bacterial cells, cellular debris, bacterial blebs, and free endotoxin.

Bispecific Antibody Construction and Tumor Targeting

Bispecific Antibody (BsAb) was constructed by linking an anti-*S*. Typhimurium O-antigen MAb (IgG1; Biodesign) and a mouse MAb directed against a cancer cell-surface receptor that is either antihuman EGFR (IgG2a; Calbiochem) or HER2/*neu* (IgG1; Serotec), or anticanine CD3 (IgG1; Serotec). Nonspecific BsAb carried an anti-CMV MAb (IgG2a; DakoCytomation). The two antibodies were crosslinked as detailed in the Supplemental Experimental Procedures online, via their Fc regions using purified recombinant protein A/G (Pierce Biotechnology), which results in BsAb as well as multimeric complexes. The BsAb was incubated with minicells for 1 hr at room temperature to enable BsAb binding to the minicell surface exposed O-polysaccharide. Excess unbound BsAb was removed by filtration through 0.2 μm filter (PALL). Approximately 5 μg of the BsAb complex was sufficient to saturate 10^9 minicells.

Cancer Cell Lines and Drug Packaging in Minicells

Chemotherapeutic drugs, Dox and Pac, were dissolved in sterile physiological saline and in 50:50 (v:v) Cremophor EL:ethanol, respectively (Sigma). Pac solution was diluted 1:5 in 0.9% saline immediately before injection. MDA-MB-468 breast, SKOV-3 ovarian, A549 lung, and HL-60 promyelocytic leukemia cancer cell lines (ATCC) were cultured in RPMI-1640 medium (Gibco) supplemented with 10% FBS, 2 mM L-glutamine, and 100 U/ml of both penicillin G and streptomycin. Liposomal-Dox (DOXIL) was purchased from Ortho Biotech. Purified minicells were packaged with chemotherapeutic drugs by incubating minicells at 37°C overnight with each drug, where the external loading concentration ranged from 10 to 400 μg/ml. Oregon Green 488-conjugated Pac and BODIPY FL-conjugated vinblastine were initially dissolved in ethanol and methanol, respectively, followed by dilution in BSG. Post-drug loading into minicells, excess drug was removed by Amicon stirred-cell ultrafiltration (Millipore; 300 kDa cut-off filter) with six washes of sterile BSG. Drug extraction from packaged minicells involved five cycles of vortexing and sonication in the presence of 97 mM HCl-isopropyl alcohol (HCl-IPA). The samples were then diluted in an equal volume of water and the five cycles were repeated. After centrifugation at 13,200 rpm for 5 min to pellet debris, the supernatants were harvested for drug quantitation, as detailed in the Supplemental Experimental Procedures online.

Electron and Fluorescence Microscopy of Minicells

*min*CDE− mutant bacterial strains and purified minicells were processed for scanning and transmission EM using established protocols. Sections for TEM were visualized using a Hitachi H-7000 transmission electron microscope (ICPMR, Westmead Hospital, Sydney, Australia). Digital images were recorded using an AnalySis MegaView II widefield CCD camera. SEM specimens were examined using a Hitachi S-900 Field Emission scanning electron microscope. Samples were processed for immunogold-TEM using the freeze-substitution method (Riegman et al., 1988) and labeling minicells with anti-*S*. Typhimurium O-antigen (Factor 4, Group B specificity; Abbott Murex) mAb (1:200), followed by gold (10 nm)-conjugated secondary antibody. Samples were analyzed using a Philips CM-120 BioTWIN electron microscope at 80 kV. Images were captured onto type 4489 Kodak EM emulsion film. Fluorescence microscopy images of Minicells were captured using a Leica DMLB fluorescent microscope with an Olympus DP70 camera and DP controller/camera software. Pac fluorescence was viewed using the Leica GFP filter. Images showing the minicell-cancer cell interactions were captured using the IX81 confocal microscope (Olympus) and the CellR software.

Drug Quantitation Using HPLC, LC-MS, and ICP-MS

Drugs extracted from minicells were quantitated based on HPLC-fluorescence peak and LC-MS/MS or ICP-MS (Inductively coupled plasma mass spectrometry) analyses as previously described for Dox (Zheng et al., 2001; Cummings, 1985) and Pac (Sharma et al., 1997; Larson et al., 2003). HPLC analysis was performed on a Shimadzu 10AVP system incorporating a RF-10A XL fluorescence detector. Detailed extraction, analysis, and quantitation procedures for Dox, irinotecan, cisplatin, and Pac are provided in the Supplemental Experimental Procedures online.

In Vitro Cytotoxicity Assay and Tumor Xenograft Studies in Nude Mice

In vitro cytotoxicity was evaluated using the CellTiter 96 Aqueous One Solution Cell Proliferation Assay (Promega), according to the manufacturer's instructions. Athymic (*nu/nu*) mice (4–6 weeks old) were purchased from the Animal Resources Centre, Perth, WA, and all animal experiments were performed in compliance with National Health and Medical Research Council, Australia, guidelines for the care and use of laboratory animals and with EnGeneIC Animal Ethics Committee approval. MDA-MB-468, SKOV-3, A549, and HL-60 human tumor cell lines were cultured and 1.5×10^6 cells in 50 μl serum-free media together with 50 μl growth-factor-reduced matrigel (BD Biosciences) were injected subcutaneously between the shoulder blades. Tumor volume (mm^3) was determined by measuring length (l) and width (w) and calculating volume ($V = lw^2/2$) as described (Sun et al., 1999). Experimental and control treatments were carried out once the tumor volumes were between 50 and 80 mm^3, at which time the tumor mass was clearly palpable and vascularized as determined following excision and microscopic observation of tumors. Mice were randomized to different groups prior to various treatments. All tumor volume measurements were performed by an investigator who was blinded to the treatments administered. Statistical analysis was performed by analysis of variance (ANOVA), with $p < 0.05$ being considered significant.

Minicell Biodistribution in Mice, Case Studies in NHL Dogs, and Minicell Safety Studies in Pigs

Biodistribution of minicells$_{Dox}$ was determined in two separate experiments in mice with MDA xenografts. When the tumor volume reached 140–170 mm^3 (experiment 1) or 400–600 mm^3 (experiment 2), mice were randomly divided into three groups (G1, G2, and G3) of nine mice per group, which received i.v. either free Dox (150 μg/dose), minicells$_{Dox}$ or ^{EGFR}minicells$_{Dox}$ (~74 μg Dox/dose contained in 5 × 10^9 minicells), respectively. Posttreatment, three mice from each group were euthanized at 6 and 24 hr and plasma and tissue was harvested, frozen, and lyophilized for extraction and determination of Dox concentration using ESI and Maldi and LC-MS/MS as detailed in the Supplemental Experimental Procedures online. Biodistribution of minicells was determined by radioiodinating anti-EGFR/anti-LPS or anti-CMV/anti-LPS BsAbs prior to minicell surface O-polysaccharide attachment. The minicells were administered i.v. into nude mice bearing MDA-MB-468 xenografts. Five mice from each group were euthanized at 2, 6, and 24 hr posttreatment and tumor, spleen, liver, kidney, and lungs were excised from each mouse. The organs were washed in sterile saline and weighed, and radioactivity was determined using a Wallac Wizard 1470 Automatic Gamma Counter. Detailed methods are described in the Supplemental Experimental Procedures online.

Two dogs with biopsy-proven T cell NHL were treated with ^{CD3}minicells$_{Dox}$, which targeted the canine CD3 T cell surface receptor as detailed in the Supplemental Experimental Procedures online. The dogs were treated at the Brisbane Veterinary Specialist Centre (Australia) with the owners' consent.

The safety of minicells was determined in three large white Landrey × Durock pigs that were given ~5 × 10^9 minicells i.v. through ear vein catheter as detailed in the Supplemental Experimental Procedures online. The study was carried out at the University of Sydney with the approval of the animal ethics committee.

Supplemental Data

The Supplemental Data include Supplemental Experimental Procedures and three supplemental tables and can be found with this article online at http://www.cancercell.org/cgi/content/full/11/5/431/DC1/.

ACKNOWLEDGMENTS

Part of the work was supported by Biotechnology Innovation Fund (BIF) grant from AusIndustry, Australia and Proof-of-concept grant (Department of State and Regional Development, NSW, Australia). We appreciate the expert assistance of Veronika Langova (BVSC) in the two dog case studies. We appreciate the assistance of Jike Lu for preparation of samples for EM and Ross Boadle (Westmead Hospital) for processing and recording EM images.

Received: June 20, 2006
Revised: December 3, 2006
Accepted: March 15, 2007
Published: May 7, 2007

REFERENCES

Brannon-Peppas, L., and Blanchette, J.O. (2004). Nanoparticle and targeted systems for cancer therapy. Adv. Drug Deliv. Rev. *56*, 1649–1659.

Cory, A.H., Owen, T.C., Barltrop, J.A., and Cory, J.G. (1991). Use of an aqueous soluble tetrazolium/formazan assay for cell growth assays in culture. Cancer Commun. *3*, 207–212.

Cummings, J. (1985). Method for determination of 4′-deoxydoxorubicin, 4′-deoxydoxorubicinol and their 7-deoxyaglycones in human serum by HPLC. J. Chromatogr. *341*, 401–409.

De Boer, P.A., Crossley, R.E., and Rothfield, L.I. (1989). A division inhibitor and a topological specificity factor coded for by the minicell locus determine proper placement of the division septum in *E. coli*. Cell *56*, 641–649.

Denyer, S.P., and Maillard, J.-Y. (2002). Cellular impermeability and uptake of biocides and antibiotics in Gram-negative bacteria. J. Appl. Microbiol. (*Suppl. 92*), 35S–45S.

Duncan, R. (2003). The dawning era of polymer therapeutics. Nat. Rev. Drug Discov. *2*, 347–360.

Ewesuedo, R.B., and Ratain, M.J. (2003). Systemically administered drugs. In Drug Delivery Systems in Cancer Therapy, D.M. Brown, ed. (Totowa, NJ: Humana Press), pp. 3–14.

El-Rayes, B.F., and LoRusso, P.M. (2004). Targeting the epidermal growth factor receptor. Br. J. Cancer *91*, 418–424.

Ferrari, M. (2005). Cancer nanotechnology: Opportunities and challenges Nature Rev. Cancer *5*, 161–171.

Gao, X., Cui, Y., Levenson, R.M., Chung, L.W., and Nie, S. (2004). *In vivo* cancer targeting and imaging with semiconductor quantum dots. Nat. Biotechnol. *22*, 969–976.

Hobbs, S.K., Monsky, W.L., Yuan, F., Roberts, W.G., Griffith, L., Torchilin, V.P., and Jain, R.K. (1998). Regulation of transport pathways in tumor vessels: Role of tumor type and microenvironment. Proc. Natl. Acad. Sci. USA *95*, 4607–4612.

Izumi, Y., Xu, L., di Tomaso, E., Fukumura, D., and Jain, R.K. (2002). Tumour biology: Herceptin acts as an anti-angiogenic cocktail. Nature *416*, 279–280.

Jun, Y.J., Kim, J.I., Jun, M.J., and Sohn, Y.S. (2005). Selective tumor targeting by enhanced permeability and retention effect. Synthesis and antitumor activity of polyphosphazene-platinum (II) conjugates. J. Inorg. Biochem. *99*, 1593–1601.

Langer, R. (1998). Drug delivery and targeting. Nature *392*, 5–10.

Larson, R.L., Khazaeli, M.B., and Dillion, H.K. (2003). Development of an HPLC method for simultaneous analysis of five antineoplastic agents. Appl. Occup. Environ. Hyg. *18*, 109–119.

Lutkenhaus, J., and Addinall, S.G. (1997). Bacterial cell division and the Z ring. Annu. Rev. Biochem. *66*, 93–116.

Ma, L., King, G.F., and Rothfield, L. (2004). Positioning of the MinE binding site on the MinD surface suggests a plausible mechanism for activation of the *Escherichia coli* MinD ATPase during division site selection. Mol. Microbiol. *54*, 99–108.

Mamot, C., Drummond, D.C., Greiser, U., Hong, K., Kirpotin, D.B., Marks, J.D., and Park, J.W. (2003). Epidermal growth factor receptor (EGFR)-targeted immunoliposomes mediate specific and efficient drug delivery to EGFR- and EGFRvIII-overexpressing tumor cells. Cancer Res. *63*, 3154–3161.

Mattick, K.L., Jorgensen, F., Legan, J.D., Cole, M.B., Porter, J., Lappin-Scott, H.M., and Humphrey, T.J. (2000). Survival and filamentation of *Salmonella enterica* serovar Enteritidis PT4 and *Salmonella enterica* serovar Typhimurium DT104 at low water activity. Appl. Environ. Microbiol. *66*, 1274–1279.

Medina, O.P., Zhu, Y., and Kairemo, K. (2004). Targeted liposomal drug delivery in cancer. Curr. Pharm. Des. *10*, 2981–2989.

Myers, M.J., Farrell, D.E., Palmer, D.C., and Post, L.O. (2003). Inflammatory mediator production in swine following endotoxin challenge with or without co-administration of dexamethasone. Int. Immunopharmacol. *3*, 571–579.

Nicholson, R.I., Gee, J.M., and Harper, M.E. (2001). EGFR and cancer prognosis. Eur. J. Cancer *37*, S9–S15.

Nielsen, U.B., Kirpotin, D.B., Pickering, E.M., Hong, K., Park, J.W., Refaat Shalaby, M., Shao, Y., Benz, C.C., and Marks, J.D. (2002). Therapeutic efficacy of anti-ErbB2 immunoliposomes targeted by a phage antibody selected for cellular endocytosis. Biochim. Biophys. Acta *1591*, 109–118.

Nikaido, H. (2003). Molecular basis of bacterial outer membrane permeability revisited. Microbiol. Mol. Biol. Rev. *67*, 593–656.

Nikaido, H. (1996). Multidrug efflux pumps of gram-negative bacteria. J. Bacteriol. *178*, 5853–5859.

Petit, A.M., Rak, J., Hung, M.C., Rockwell, P., Goldstein, N., Fendly, B., and Kerbel, R.S. (1997). Neutralizing antibodies against epidermal growth factor and ErbB-2/*neu* receptor tyrosine kinases down-regulate vascular endothelial growth factor production by tumor cells *in vitro* and *in vivo*: Angiogenic implications for signal transduction therapy of solid tumors. Am. J. Pathol. *151*, 1523–1530.

Piddock, L.J.V. (2006). Multidrug-resistance efflux pumps — not just for resistance Nature Rev. Microbiol. *4*, 629–636.

Poole, K. (2002). Outer membranes and efflux: The path to multidrug resistance in Gram-negative bacteria. Curr. Pharm. Biotechnol. *3*, 77–98.

Rae, J.M., and Lippman, M.E. (2004). Evaluation of novel epidermal growth factor receptor tyrosine kinase inhibitors. Breast Cancer Res. Treat. *83*, 99–107.

Riegman, N., van Die, I., Leunissen, J., Hoekstra, W., and Bergmans, H. (1988). Biogenesis of F7(1) and F7(2) fimbriae of uropathogenic *Escherichia coli*: Influence of the FsoF and FstFG proteins and localization of the Fso/FstE protein. Mol. Microbiol. *2*, 73–80.

Saleh, M.N., Sugarman, S., Murray, J., Ostroff, J.B., Healey, D., Jones, D., Daniel, C.R., LeBherz, D., Brewer, H., Onetto, N., et al. (2000). Phase I trial of the anti-Lewis Y drug immunoconjugate BR96-doxorubicin in patients with Lewis Y-expressing epithelial tumors. J. Clin. Oncol. *18*, 2282–2292.

Schulz, G.E. (1993). Bacterial porins: Structure and function. Curr. Opin. Cell Biol. *5*, 701–707.

Sharma, A., Mayhew, E., Bolcsak, L., Cavanaugh, C., Harmon, P., Janoff, A., and Bernacki, R.J. (1997). Activity of paclitaxel liposome formulations against human ovarian tumor xenografts. Int. J. Cancer *71*, 103–107.

Shizuo, A., and Takeda, K. (2004). Toll-like receptor signaling. Nat. Rev. Immunol. *4*, 499–511.

Sievers, E.L., Larson, R.A., Stadtmauer, E.A., Estey, E., Lowenberg, B., Dombret, H., Karanes, C., Theobald, M., Bennett, J.M., Sherman, M.L., et al. (2001). Efficacy and safety of gemtuzumab ozogamicin in patients with CD33-positive acute myeloid leukemia in first relapse. J. Clin. Oncol. *19*, 3244–3254.

Slamon, D.J., Clark, G.M., Wong, S.G., Levin, W.J., Ullrich, A., and McGuire, W.L. (1987). Human breast cancer: Correlation of relapse and survival with amplification of the HER-2/*neu* oncogene. Science *235*, 177–182.

Sun, J., Blaskovich, M.A., Knowles, D., Qian, Y., Ohkanda, J., Bailey, R.D., Hamilton, A.D., and Sebti, S.M. (1999). Antitumor efficacy of a novel class of non-thiol-containing peptidomimetic inhibitors of farnesyltransferase and geranylgeranyltransferase I: Combination therapy with the cytotoxic agents cisplatin, taxol and gemcitabine. Cancer Res. *59*, 4919–4926.

Van den Berg, B., Black, P.N., Clemons, W.M., Jr., and Rapoport, T.A. (2004). Crystal structure of the long-chain fatty acid transporter FadL. Science *304*, 1506–1509.

Van den Berg, B. (2005). The FadL family: Unusual transporters for unusual substrates. Curr. Opin. Struct. Biol. *15*, 401–407.

Yuan, F., Salehi, H.A., Boucher, Y., Vasthare, U.S., Tuma, R.F., and Jain, R.K. (1994). Microvascular permeability and interstitial penetration of sterically stabilized (stealth) liposomes in a human tumor xenograft. Cancer Res. *54*, 3352–3356.

Zheng, J.H., Chen, C.T., Au, J.L., and Wientjes, M.G. (2001). Time- and concentration- dependent penetration of doxorubicin in prostrate tumours. AAPS PharmSci. *3*, e15. 10.1208/ps030215.